

Near-infrared spectroscopy of the LMC recurrent nova LMCN 1968-12a

A. Evans,^{1*} D. P. K. Banerjee², T. R. Geballe³, A. Polin⁴, E. Y. Hsiao⁵,
K. L. Page⁶, C. E. Woodward⁷, S. Starrfield⁸

¹*Astrophysics Group, Lennard Jones Laboratory, Keele University, Keele, Staffordshire, ST5 5BG, UK*

²*Physical Research Laboratory, Navrangpura, Ahmedabad, Gujarat 380009, India*

³*Gemini Observatory/NSF's NOIRLab, 670 N. Aohoku Place, Hilo, HI, 96720, USA*

⁴*Department of Physics and Astronomy, Purdue University, 525 Northwestern Avenue, West Lafayette, IN 47907, USA*

⁵*Department of Physics, Florida State University, 77 Chieftan Way, Tallahassee, FL 32306, USA*

⁶*School of Physics and Astronomy, University of Leicester, University Road, Leicester, LE1 7RH, UK*

⁷*Minnesota Institute for Astrophysics, School of Physics & Astronomy, 116 Church Street SE, University of Minnesota, Minneapolis, MN 55455, USA*

⁸*School of Earth and Space Exploration, Arizona State University, Box 876004, Tempe, AZ 85287-6004, USA*

Accepted XXX. Received YYY; in original form ZZZ

ABSTRACT

We have obtained near-infrared (0.80–2.45 μm) spectra of the recurrent nova LMCN 1968-12a on two occasions during its 2024 August eruption. This is the first near-infrared spectroscopy of an extragalactic nova. The initial spectrum, on day 8.48, caught the nova in the coronal phase, with the [Si x] 1.43 μm line being extremely strong. This line had a luminosity of $\sim 95 L_{\odot}$, and is clearly a very powerful coolant. Its presence, together with the absence of [Si ix] 1.56 μm , implies a coronal temperature $\gtrsim 3 \times 10^6$ K, possibly amongst the highest recorded coronal temperature in a nova eruption. With the exception of the [Si x] line, the near-infrared spectra are remarkable for being devoid of metal lines. We suggest that this is due, in part, to the exceptionally high temperature of the coronal gas, causing ions, whose emission lines would normally appear in the near-infrared spectrum, to be collisionally ionised to higher stages.

Key words: stars: individual: Nova LMC 2024 – novae, cataclysmic variables – infrared: stars – ultraviolet: stars – transients: novae

1 INTRODUCTION

Nova explosions occur in semi-detached binary systems containing a late-type star (the secondary) and a white dwarf (WD). Material from the secondary spills onto the WD via an accretion disc. In time, conditions at the base of the layer accreted on the WD become degenerate, and hot enough to trigger a thermonuclear runaway (TNR). This produces a nova eruption, leading to the violent ejection of material, at several hundred to several thousand kms^{-1} . Once the eruption has subsided, accretion resumes and in time, another eruption occurs: all novae are recurrent. However the eruptions of *recurrent* novae (RNe) repeat on time-scales $\lesssim 100$ yr (see Anupama 2008; Darnley & Henze 2020; Darnley 2021, for reviews).

RNe are defined by the selection effect that the sys-

tem has been observed to have undergone more than one TNR. Fewer than a dozen Galactic RNe are known. There are rather more extragalactic RNe; the majority of these are in M31. There are also four in the Large Magellanic Cloud (LMC) (Healy-Kalesh et al. 2024). The second eruption in the LMC of “Nova Mensae 1968” in 1990 (Liller 1990) meant that this object was the first extragalactic RN to be observed; its most recent eruption occurred in 2024 August.

We present here near infrared (NIR) 0.8–2.5 μm spectroscopy of the 2024 eruption, the first NIR spectroscopic study of any extragalactic RN. A preliminary account was given by Banerjee et al. (2024).

2 THE LMC SYSTEM

Previous eruptions of Nova LMC 1968 were observed in 1968, 1990 (Shore et al. 1991), 2002, 2010 (Mróz et al. 2014), 2016 (Mróz & Udalski 2016; Kuin et al. 2020), and 2020.

* E-mail: a.evans@keele.ac.uk

A comprehensive discussion of these eruptions is given by [Kuin et al. \(2020\)](#), who concluded that it is unlikely that other eruptions had occurred since 1999. The nova is known in the literature as LMCN 1968-12a, LMCN 1990-02a, LMCN 2010-11a, LMCN 2016-01, Nova LMC 1990b, OGLE 2016-NOVA-1, and LMC V1341. We refer to it here as LMC68.

LMC68 has an orbital period of 1.26432 d ([Mróz et al. 2014](#)), suggesting that it is a RN of the “U Sco” type (e.g. [Anupama 2008](#)). The similarities between LMC68 and U Sco have been discussed by [Kuin et al. \(2020\)](#). Unlike RNe with red giant (RG) secondaries, there is no RG wind in U Sco-type RNe with which the ejected material interacts. The comparable orbital periods suggests that the secondary in LMC68 is similar to that in the U Sco system, in which the secondary is a sub-giant ([Anupama 2008](#)).

[Kuin et al. \(2020\)](#) give the *VI* magnitudes in quiescence from the OGLE survey ([Mróz et al. 2014](#)) as $\langle V \rangle = 19.70$, $\langle I \rangle = 19.29$. Assuming a range of ± 0.5 in these values (see Figure 5 of [Mróz et al. 2014](#)), these data are consistent with a black body with temperature ~ 6700 K and luminosity $\sim 30 L_{\odot}$, although in view of the paucity of, and nature of, the data, these values are subject to significant uncertainties (see Fig. 5 below).

There appear to be no deep NIR images of the nova field, and it is not resolved in the Two Micron All Sky Survey (2MASS; [Skrutskie et al. 2006](#)). However, it was observed in the *Y*, *J*, and *K_s* bands by the Visible and Infrared Survey Telescope for Astronomy (VISTA; [Cioni et al. 2011](#)) in 2014 November, when the system was in quiescence. We reproduce the *Y* band image in Fig. 1 as it provides a useful finder for NIR observations.

We assume the distance and reddening to LMC68 to be 50 kpc ([Pietrzyński et al. 2019](#)), and $E(B - V) = 0.07$ ([Kuin et al. 2020](#)) respectively.

3 THE 2024 ERUPTION

Following the 2020 eruption, a recurrence period of four years was proposed ([Page, Kuin & Darnley 2020](#)). Right on cue, LMC68 erupted in 2024 August ([Darnley et al. 2024](#); [Stubbings 2024](#)). The Neil Gehrels Swift Observatory ([Gehrels et al. 2004](#)) had been monitoring LMC68 with monthly cadence since the end of the 2020 eruption. A Swift observation comprised of two “snapshots” taken some 16 hrs apart, was obtained on 2024 August 1. LMC68 was still in quiescence during the first snapshot (obtained on August 1.19 UT), but clearly in eruption during the second (August 1.83 UT). The 2024 eruption therefore occurred between (UT) August 1.19 (MJD 60523.19) and August 1.83 (MJD 60523.83). We take zero of time from the latter, $t_0 = \text{MJD } 60523.83$.

Optical spectroscopy covering the wavelength range 3600–7800 Å was obtained on day 4.7 ([Shore et al. 2024](#)), when He II 4686 Å dominated the spectrum. H α had broad wings extending to $\pm 5000 \text{ km s}^{-1}$. Most interestingly, [Shore et al.](#) note that there were no metal lines present. They also found that the emission line profiles differed from those presented by [Kuin et al. \(2020\)](#), suggesting that the ejecta morphology may differ from eruption to eruption, or that there may be orbital phase effects ([Kuin et al. 2020](#)).

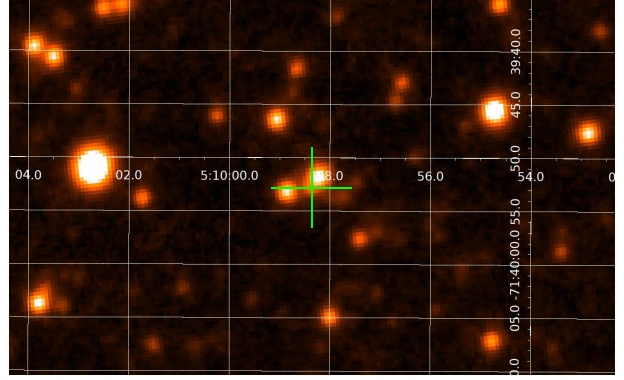


Figure 1. NIR field of LMC68. *Y* image from the VISTA survey. LMC68 is located at the centre of the green cross; it is $\sim 1''5$ SE of a brighter star.

Swift observations obtained on day 7.8 revealed a soft X-ray source ([Page, Kuin & Darnley 2024](#)), which was approximated by black body emission with temperature T_{Swift} given by $kT_{\text{Swift}} = 71^{+28}_{-50}$ eV; a deeper observation on the following day gave $kT_{\text{Swift}} = 66 \pm 12$ eV.

4 OBSERVATIONS

4.1 Magellan

A low resolution spectrum covering the wavelength range 0.8–2.5 μm was obtained on 2024 August 10.41 UTC (MJD 60532.41 = day 8.58) at a mean airmass of 1.502, with the Folded Port Infrared Echellette (FIRE) spectrograph on the 6.5 m Magellan Baade Telescope ([Simcoe et al. 2008](#)). The observation consisted of standard ABBA loops on LMC68, followed immediately by an observation of the telluric standard HD 223296.

The resolving powers, R , were 500 in the *J* band, 450 (*H*), and 300 (*K*). The spectrum was reduced using a custom IDL package ([Simcoe et al. 2008](#)) and additional procedures described by [Hsiao et al. \(2019\)](#).

4.2 Gemini-S

NIR spectra covering 0.90–2.45 μm were obtained at Gemini South on 2024 August 24.32 (MJD 60546.318 = day 22.49). The facility instrument Flamingos-2 ([Eikenberry et al. 2004](#)) was used and was configured with its $0''.72$ wide slit and its *JH* (covering 0.9–1.75 μm) and *HK* (1.54–2.45 μm) grisms. With this slit width the resolving power of the *JH* grism varies from ~ 200 to ~ 700 across its wavelength range, and that of the *HK* grism varies from ~ 300 to ~ 700 across its wavelength range¹. Spectra were obtained in the standard ABBA mode with a nod angle of $6''$. Total exposure times were 1,440 seconds and 2,400 seconds for the short and long wavelength segments, respectively. The time intervals for the observations were UT 06.99–07.47 hr for *JH* and UT 07.74–08.55 hr for *HK*. The mean airmass was 1.70 for the *JH* segment and 1.55 for the *HK* segment. The A0V stars HIP 18842 and HIP 30360 were employed as telluric standards for *JH* and *HK*, respectively. The mean times of the (short) telluric standard observations

¹ See <https://www.gemini.edu/instrumentation/flamingos-2/components#Grisms>.

were UT 06.43 (*JH*) and UT 08.97 (*HK*). Data reduction incorporated both IRAF and Figaro routines as described in Evans et al. (2022). Because of large difference in the OH sky line emission line brightnesses between the A and B spectra during the *HK* measurements, it was necessary to scale the *HK* spectra in the A position by a factor of 0.9 before combining them with the spectra in the B position. This procedure removed the residual sky lines. The *HK* spectrum was then scaled to match the *JH* spectrum in their overlapping wavelength interval (1.50–1.75 μm) and both spectra were resampled in bins of 0.002 μm , prior to adjoining them.

The Magellan and Gemini spectra are shown in Fig. 2. All wavelengths are vacuum values. The Magellan (day 8.58) data are shown up to 2.0 μm only, as the data longward of this have low signal-to-noise ratio ($\lesssim 3$).

4.3 Swift

LMC68 was observed with the Swift X-ray telescope (XRT) at times close to those of the NIR observations:

- (i) on MJD 60533.692 (day 9.86), the data are fitted by a super soft X-ray source with temperature $kT_{\text{Swift}} = 49_{-8}^{+11}$ eV, $T_{\text{Swift}} = 5.7_{-0.9}^{+1.3} \times 10^5$ K, and
- (ii) on MJD 60546.420 (day 22.59), with $kT_{\text{Swift}} = 122 \pm 10$ eV, $T_{\text{Swift}} = 1.41 \pm 0.12 \times 10^6$ K.

Following the discovery of the 2024 eruption by Swift, a daily monitoring campaign was initiated. The data were processed and analysed using HEASOFT v6.34², together with the most recent calibration files available at the time.

LMC68 was also observed with the UV/Optical telescope UVOT. The UVOT magnitudes are listed in Table 1, together with the corresponding fluxes based on the calibration given in Breeveld et al. (2011). The entire Swift dataset will be published elsewhere.

5 DESCRIPTION OF SPECTRA

5.1 Day 8.58

The day 8.58 spectrum shows the coronal line [Si x] 1.4305 μm to be extraordinarily strong (see Fig. 2). The dereddened flux is $f = [1.22 \pm .01] \times 10^{-15}$ W m⁻², which translates to $\sim 95 L_{\odot}$. This is significantly greater than the [Si x] 1.43 μm flux in U Sco at the same time post eruption ($\sim 1.5 L_{\odot}$; Evans et al. 2023, see Fig. 6 below), and much larger than the highest measured [Si x] flux in the nova V1674 Her ($\sim 23 L_{\odot}$; Woodward et al. 2021). The line is clearly a very powerful coolant of the coronal gas. Following Woodward et al. (2021), kT_* defines the temperature T_* at which half the photons emitted by the corresponding blackbody are capable of ionising the lower ion ($kT_* \simeq 0.426 \times$ ionisation potential). For [Si x], $kT_* = 146$ eV, and as the temperature of the X-ray-emitting gas was $kT_{\text{Swift}} \simeq 49$ eV, it seems unlikely that the Si was photo-ionised.

[Si IX] 1.5560 μm ($kT_* = 127$ eV) is often seen in the wavelength range covered by the Magellan data, but it is not present, to a 3σ limit of $\sim 1.9 \times 10^{-16}$ W m⁻². The

presence of [Si x] 1.4305 μm , coupled with the absence of [Si IX] 1.5600 μm , may be used to estimate the temperature of the coronal gas, using (e.g., Greenhouse et al. 1990)

$$\frac{f([\text{Si IX}])}{f([\text{Si x}])} = \frac{n(\text{Si IX})}{n(\text{Si x})} \frac{\lambda([\text{Si x}])}{\lambda([\text{Si IX}])} \frac{\Upsilon(\text{Si IX})}{\Upsilon(\text{Si x})} \frac{g_l(\text{Si x})}{g_l(\text{Si IX})},$$

where n is the number density of each ion, Υ is the effective collision strength (i.e. the collisional strength averaged over a thermal electron distribution), and g_l is the statistical weight of the lower level. The apparent absence of [Si IX] 1.5600 μm suggests that the temperature of the coronal gas was $T_{\text{cor}} \gtrsim 10^{6.45}$ K ($\sim 3 \times 10^6$ K). We have used the values of Υ from the IRON Project online database³ (Hummer et al. 1993; Badnell et al. 2006); we have taken the temperature-dependence of Υ for [Si IX], and the value at 10^5 K (the highest temperature available) for [Si IX]. We have also used ionisation data from Arnaud & Rothenflug (1985).

The time by which the NIR coronal lines appeared in LMC68 following its 2024 eruption (i.e., $t < 8.58$ d) is comparable to that seen in other “fast” novae⁴ (9.41 d and 11.51 d in U Sco and V1674 Her respectively; Woodward et al. 2021; Evans et al. 2023). This suggests that the early ($\lesssim 10$ days) appearance of NIR coronal lines during nova eruptions (both classical and recurrent) is not unusual in fast novae. However, the coronal phase in slower novae may occur much later (see the compilation in Table VIII of Benjamin & Dinerstein 1990).

Also present, but far weaker, are Pa β 1.2818 μm , He I 1.0833 μm , He II 5-4 1.0126 μm , and He II 7-5 1.163 μm . The dereddened flux ratio $f(\text{He II 7-5})/f(\text{He II 5-4})$ is approximately 0.2. Assuming that Case B (Storey & Hummer 1995) applies to the He II-bearing gas, this flux ratio is consistent with a range of electron densities ($10^3 < n_e \text{ (cm}^{-3}\text{)} < 10^{10}$) and electron temperatures ($5000 < T_e \text{ (K)} < 10^5$).

Both [Si x] and He I are double-peaked on day 8.58, with half width at zero intensity (HWZI) ~ 5000 km s⁻¹ and separation between peaks of ~ 5000 km s⁻¹ (see Fig. 3); this is broadly similar to the H α profile on day 4.7 (Shore et al. 2024), although the latter had a narrow central portion in the velocity range -900 km s⁻¹ to 1780 km s⁻¹. While the profiles of [Si x] and He I are similar, it is unlikely that they arise in the same region of the ejecta, for reasons discussed below. The high velocity and the profile suggest that, as in U Sco, they arise in collimated outflows ejected orthogonal to the binary plane (Evans et al. 2023). The high inclination of the binary (Kuin et al. 2020) suggests that the ejected velocity is much higher than this. The critical electron density for the [Si x] 1.4305 μm transition (above which the upper level is collisionally rather than radiatively de-excited) is $n_{\text{crit}} \simeq 2.76 \times 10^5 T_e^{1/2} \text{ cm}^{-3}$, where T_e is the electron temperature. From the silicon coronal lines ([Si x] 1.4305 μm , [Si IX] 1.5600 μm), we determined that $T_{\text{cor}} \gtrsim 3 \times 10^6$ K, so that $n_{\text{crit}} \gtrsim 4.9 \times 10^8 \text{ cm}^{-3}$ if $T_{\text{cor}} = T_e$. The [Si x] 1.4305 μm and He II lines can be co-spatial if the electron density in this region is $\lesssim 10^8 \text{ cm}^{-3}$.

Both Pa β and He II 5-4 are present in the day 8.58 data. For both lines the upper level is $n = 5$, so the expected

³ <http://cdsweb.u-strasbg.fr/tipbase/home.html>

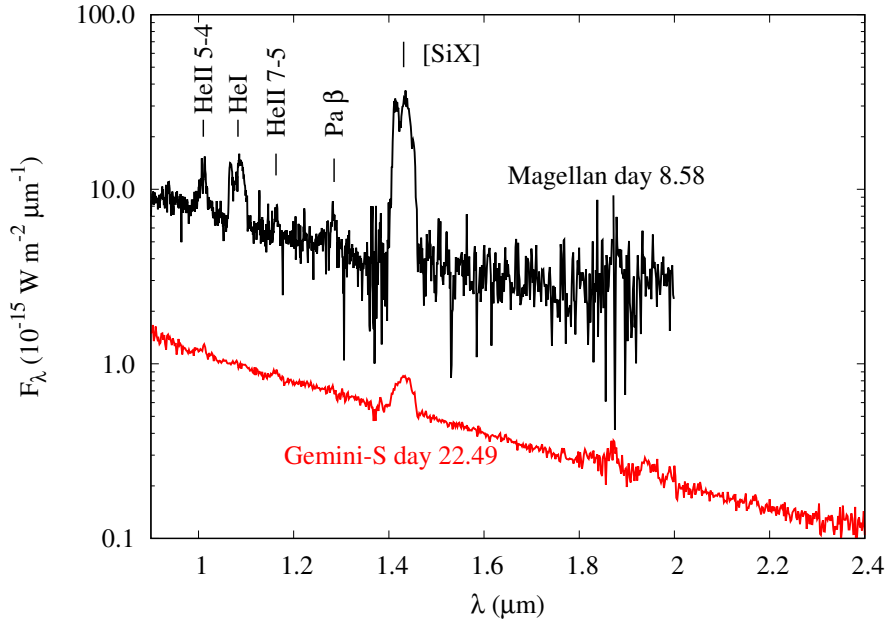
⁴ Novae whose visual light curves decline by 2 magnitudes on a time-scale $\lesssim 20$ days (Warner 2012).

² <https://heasarc.gsfc.nasa.gov/docs/software/heasoft/>

Table 1. Observed UVOT fluxes*.

Filter	λ (\AA)	MJD	Mag	Flux ($10^{-14} \text{ W m}^{-2} \mu\text{m}^{-1}$)
<i>v</i>	5410	60533.0979	16.694 ± 0.093	0.78 ± 0.07
<i>b</i>	4321	60533.0925	16.752 ± 0.054	1.29 ± 0.06
<i>u</i>	3442	60533.0914	15.569 ± 0.044	2.09 ± 0.08
<i>w1</i>	2486	60533.0897	15.295 ± 0.041	3.03 ± 0.11
<i>m2</i>	2221	60533.0998	15.067 ± 0.045	4.36 ± 0.18
<i>w2</i>	1991	60533.0952	15.060 ± 0.032	5.06 ± 0.15
<i>w2</i>	1991	60533.6903	15.519 ± 0.048	3.32 ± 0.15
<i>w2</i>	1991	60533.7526	15.437 ± 0.044	3.58 ± 0.14
<i>w2</i>	1991	60533.9462	15.050 ± 0.037	5.11 ± 0.18
<i>u</i>	3442	60546.4252	15.922 ± 0.054	1.51 ± 0.08
<i>u</i>	3442	60546.4860	15.984 ± 0.045	1.42 ± 0.06
<i>w1</i>	2486	60546.4239	15.468 ± 0.048	2.59 ± 0.11
<i>w1</i>	2486	60546.4837	15.474 ± 0.039	2.57 ± 0.09
<i>m2</i>	2221	60546.4217	15.229 ± 0.047	3.76 ± 0.16
<i>m2</i>	2221	60546.4800	15.317 ± 0.039	3.46 ± 0.13
<i>w2</i>	1991	60546.4273	15.183 ± 0.037	4.52 ± 0.15
<i>w2</i>	1991	60546.4897	15.362 ± 0.032	3.83 ± 0.11

*Data not dereddened.

**Figure 2.** NIR spectra of LMC68, obtained on days 8.58 (black) and 22.49 (red). The apparent emission features around 1.8–2.0 μm are telluric in origin.**Table 2.** Dereddened line fluxes. Upper limits are 3σ .

λ_c (observed) (μm)	ID	λ ID (μm)	Dereddened Flux	
			Day 8.58 ($10^{-17} \text{ W m}^{-2}$)	Day 22.49 ($10^{-18} \text{ W m}^{-2}$)
1.010	He II 5-4	1.01264	10.39 ± 0.06	1.97 ± 0.12
1.083	He I	1.08332	24.66 ± 0.02	< 0.02
1.163	He II 7-5	1.16296	2.09 ± 0.32	1.50 ± 0.07
1.285	Pa β	1.28216	3.02 ± 0.14	< 0.02
1.431	[Si x]	1.43049	122 ± 10	13.4 ± 0.2

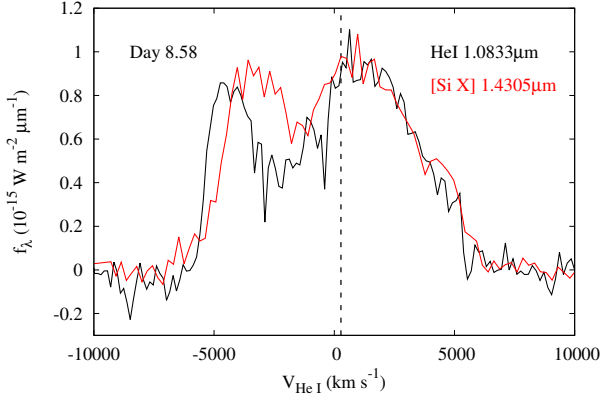


Figure 3. Line profile of the He I 1.083 μm and [Si X] 1.4305 μm features in velocity space on day 8.58 from the Magellan spectrum. The vertical dotted line is the systemic velocity of the LMC.

flux ratio has the simple form (assuming that both lines are optically thin):

$$\frac{f(\text{Pa}\beta)}{f(\text{He II})} = \frac{n(\text{H})}{n(\text{He II})} \exp\left(-\frac{3hRc}{25kT}\right) \frac{A(\text{Pa}\beta)}{A(\text{He II})} \frac{\lambda(\text{He II})}{\lambda(\text{Pa}\beta)}$$

so that

$$\frac{n(\text{He})}{n(\text{H})} = 0.1384 \exp\left(-\frac{1.894 \times 10^4}{T(\text{K})}\right) \frac{n(\text{He})}{n(\text{He II})}. \quad (1)$$

Here R is the Rydberg constant, and A is the Einstein spontaneous emission coefficient ($A = 2.201 \times 10^6 \text{ s}^{-1}$ for Pa β , $4.321 \times 10^7 \text{ s}^{-1}$ for He II 5–4). The He/H ratio by number is therefore a simple function of the temperature T (see Fig. 4), the temperature-dependence of the ratio $n(\text{He})/n(\text{He II})$ being given in Arnaud & Rothenflug (1985). If $n(\text{He})/n(\text{H}) \simeq 1$, as found by Shore et al. (1991) for the 1990 eruption, and this ratio also applies to the 2024 eruption, the implication is that He II originates in a region at $\sim 10^5 \text{ K}$ (see Fig. 4), considerably cooler than, and distinct from, the hotter ($T \simeq 10^{6.45} \text{ K}$) [Si X] 1.4305 μm emitting region. Indeed nearly all He is in the form He III above 10^5 K (Arnaud & Rothenflug 1985).

The dereddened Swift UVOT data for this epoch are consistent with a black body with a temperature of $19700 \pm 2030 \text{ K}$ and luminosity $1.8[\pm 1.0] \times 10^3 L_{\odot}$.

5.2 Day 22.49

On day 22.49, the [Si X] 1.4305 μm line was detected, but its flux had decreased by a factor ~ 100 , to $[1.34 \pm 0.02] \times 10^{-17} \text{ W m}^{-2}$. Also greatly diminished, but still present, were He II 1.0126 μm and He II 1.163 μm . However, He I 1.0833 μm and Pa β were no longer detected.

The dereddened Swift UVOT data for day 22 are consistent with a black body with temperature $20800 \pm 2400 \text{ K}$, and luminosity $\simeq [1.5 \pm 0.9] \times 10^3 L_{\odot}$ (see Fig. 5). These values are not significantly different from those apparent on day 8.58. The UVOT-derived temperatures on days 8.58 and 22.49 ($\simeq 2 \times 10^4 \text{ K}$) and bolometric luminosity ($\simeq 1.5 \times 10^3 L_{\odot}$) are remarkably similar to the same parameters obtained for U Sco during its 2022 eruption (Evans et al. 2023). The corresponding “black body angular diameter” is $\sim 0.05 R_{\odot}$. As

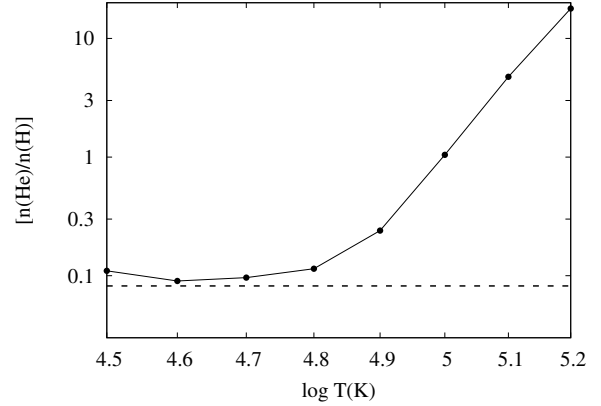


Figure 4. The He/H abundance ratio as function of temperature from, Equation (1). Horizontal dotted line is solar He/H ratio (Asplund, Amarsi & Grevesse 2021).

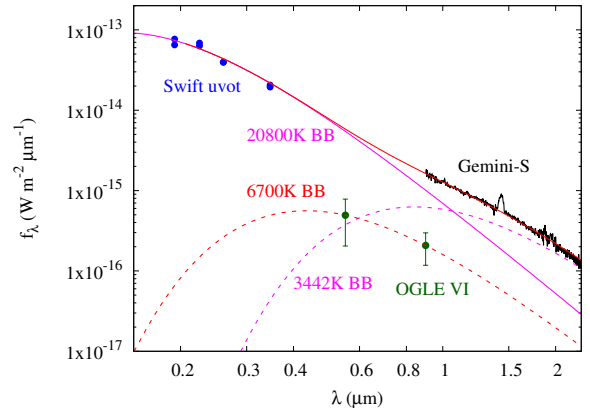


Figure 5. The UV-IR flux distribution of LMC68 on day 22.49. All data dereddened. Blue circles, Swift UVOT data; black line: Gemini-S NIR data. Full magenta curve, 20800 K black body fit to Swift data. Dotted magenta curve, 3442 K black body fit to excess as described in text. Full red curve is sum of 20800 K and 3442 K black bodies. Dotted red curve, 6700 K black body fit to OGLE data (green); see discussion in Section 2.

in the case of U Sco, we explore the possibility that this emission is due to irradiation of the secondary by the hot WD. For a secondary star of mass $\sim 1 M_{\odot}$, the Roche lobe radius is $\sim 0.2 R_{\odot}$. The formalism of Kovetz, Prialnik & Shara (1988) gives the irradiated temperature as $\sim 10^5 \text{ K}$ and luminosity $\sim 2 \times 10^4 L_{\odot}$, if the WD was radiating at the Eddington luminosity. It seems unlikely, therefore, that this emission is the result of irradiation of the secondary by the hot WD.

As shown in Fig. 5, the extrapolation of this black body to longer wavelengths reveals an excess in the NIR. A NIR wavelength excess was also evident in the outburst NIR spectrum of U Sco (Evans et al. 2023), which was attributed to free-free and free-bound emission. In the case of LMC68, however, the excess is not fitted by free-free and free-bound emission, but is consistent with black body emission at $\sim 3400 \text{ K}$ and luminosity $\sim 63 L_{\odot}$ (see Fig. 5).

5.3 Comparison with U Sco

With the limited amount of LMC68 data at our disposal, we compare LMC68 with the Galactic RN U Sco at equivalent stages of their outbursts. The latter has had RN eruptions in 1863, (1873, 1884, 1894), 1906, 1917, (1927), 1936, 1945, (1955), 1969, 1979, 1987, 1999, 2010, (2016), and 2022, dates in brackets being probable eruptions which were missed (see summary in [Evans et al. 2023](#)). The mean time between eruptions for U Sco is ~ 10 yr, of the same order as the 4-yr recurrence time for LMC68.

Fortuitously, the NIR data reported here were obtained at similar times after eruption as some of the NIR spectroscopy of the 2022 eruption of U Sco ([Evans et al. 2023](#)). To compare the data we have scaled the U Sco spectra to the LMC by applying a factor $[10/50]^2$, where the distance of U Sco is taken to be 10 kpc. The comparison is shown in Fig. 6. Given the crude nature of the scaling, the continuum levels are strikingly similar, but there are clear differences between the two objects (the day numbers below are for LMC68):

(i) Day 8.58: the earlier spectra are broadly similar, in terms of the shape of the continuum and the emission lines present. The glaring exception is the extraordinary strength of [Si x] 1.4305 μm in LMC68. Other than this line there is no clear evidence for any metal lines in the NIR spectrum.

(ii) Day 22.49: the later spectra are very different. The NIR continuum of U Sco is much bluer than that of LMC68, essentially because there is a greater contribution from the hot black body in the former. The emission lines in LMC68 are (with the exception of [Si x] 1.4305 μm) weak or non-existent, in contrast to U Sco. The absence of He I 1.0833 μm in LMC68 is intriguing, as the strength of this line in U Sco went through a flux minimum on day 23.36 ([Evans et al. 2023](#)).

6 WHERE ARE THE METAL LINES?

A striking feature of the LMC68 NIR spectra reported here, compared to the apparently similar system U Sco, is the absence of any metal lines, with the exception of the [Si x] coronal line at $\lambda = 1.4305 \mu\text{m}$. In addition to H and He lines, lines of aluminium, sulphur and calcium are generally present (e.g. [Al ix] 2.04 μm , [S ix] 1.25 μm , [Ca viii] 2.302 μm). In particular, the Al and the S lines are usually present along with the [Si x] 1.43 μm line, all the ions involved having similar ionisation potentials, in the range 300–400 eV (e.g., Table 2 in [Woodward et al. 2021](#), and [Evans et al. 2023](#)). In general, the [Al ix] 2.04 μm line is very strong, often as strong as [Si x] 1.43 μm (see, e.g., the NIR spectrum of U Sco in the right panel of Fig. 6). As noted above, an optical spectrum on day 4.7 of the 2024 eruption ([Shore et al. 2024](#)) was similarly devoid of metal lines.

In addition to the above NIR coronal lines, a number of other, weaker, coronal lines are often seen during nova eruptions, for example [P viii] 1.7361 μm , [Cr xi] 1.5503 μm , [Ti vi] 1.715 μm , and [Mn xiv] 2.092 μm ([Wagner & Depoy 1996](#); [Raj et al. 2015](#); [Gehrz et al. 2018](#); [Kumar et al. 2022](#); [Rudy et al. 2024](#)).

The issue is not solely an absence of coronal lines. NIR spectra of the 2006 eruption of the RN RS Oph have (in ad-

dition to coronal lines) O I 1.1287, 1.3164 μm , C I 1.1748 μm , and Fe II 1.6872 μm ([Banerjee, Das & Ashok 2009](#)); note that it is possible that these lines may have contributions from the RG wind.

Metal lines *have* been seen in outburst spectra of LMC68. Spectra of the 1990 eruption obtained with the International Ultraviolet Explorer (IUE) satellite ([Shore et al. 1991](#)) show N v 1240Å, Si iv 1400Å, and C iv 1500Å, all of which weakened considerably over the first ~ 10 days of the eruption. Swift UVOT grism spectra obtained during the first 10 days of the 2016 eruption ([Kuin et al. 2020](#)) showed C III 1909Å and O III 3133Å; these emission lines were rather weak.

While the NIR properties of LMC68 may merely be a consequence of its extreme nature, we consider below other possible reasons for the metal-deficient nature of the 2024 LMC68 ejecta.

6.1 Electron density

Might the electron density in the coronal region have been so high as to permit the collisional de-excitation of the transition upper levels? This is of course possible but can not explain the absence of other lines (e.g., O I 1.1287, 1.3164 μm) commonly seen in the evolution of the NIR spectra of RNe.

6.2 TNR when the secondary is metal poor

LMC68 differs from Galactic RNe in that the metallicity of the secondary is likely to be typical of the LMC. The metallicity of LMC RGs is $[\text{Fe}/\text{H}] \simeq -0.6$ ([Cole, Smecker-Hane & Gallagher 2000](#)). Nova explosions occurring in binaries in which the secondary has less-than-Solar metallicity have been discussed by [Chen et al. \(2019\)](#), [Starrfield et al. \(2000\)](#), and [José et al. \(2007\)](#). As discussed by [Starrfield et al. \(2012\)](#), the accretion of low-metallicity material on to the WD results in a more violent explosion. This is because the key driver of the TNR is the $^{12}\text{C}(p, \gamma)^{13}\text{N}$ reaction, so the lower the metallicity, the more accreted material is required to power the outburst, the greater the pressure at the base of the accreted envelope and the greater the strength of the eruption.

Even though the secondary is likely metal-deficient, the material accreted on the surface of the WD is still processed through the TNR, along with material dredged up from the WD (although the extent to which the latter would occur in an ultra-short recurrence period RN is not clear). The composition of the ejecta will therefore reflect this. Indeed, in view of the likely more energetic eruption, metals beyond Ca (the usual end-point of the TNR in nova explosions), are expected in a nova arising in a binary with a metal-deficient secondary ([José et al. 2007](#)). Although those authors considered only cases of *extreme* metal deficiency (e.g., solar/ 2×10^5), their models suggest that C, N, O, Si, Al, S, P are all expected to be enhanced relative to solar, whereas Mg and Ca are expected to be *deficient* relative to solar.

Thus, the metal-deficiency of the secondary can not by itself account for the lack of metal lines in the NIR.

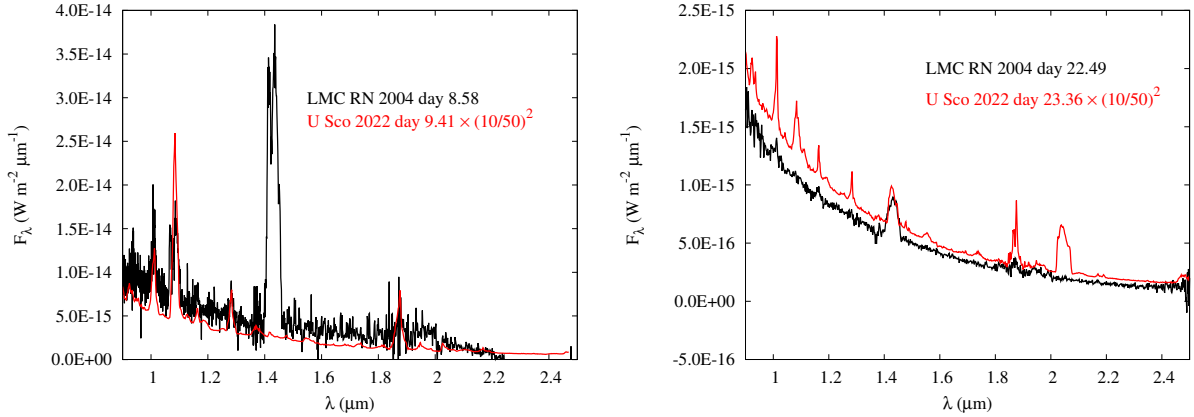


Figure 6. Comparison of the NIR spectra of LMC68 and U Sco (Evans et al. 2023), obtained at similar intervals after eruption.

6.3 Collisional ionisation

The X-ray source in LMC68 was never hot enough to ionise the gas to the extent that coronal lines would be present (kT_{Swift} was less than the ionisation potential for the lower ionisation states). The alternative is that the Si IX is produced by shocks. The fact that the secondary is not a RG means that there is little or no wind with which the nova ejecta can interact, but there might be interaction between ejected material moving at different velocities. It is known that velocities up to 5000 km s^{-1} are present (see above and Shore et al. 2024). Shore et al. also note the presence of narrower central features in the interval -900 km s^{-1} to 1780 km s^{-1} , suggesting that there are regions of the ejecta with relative velocities V_{rel} in excess of 1000 km s^{-1} . The RMS velocity V_{rms} of a gas, even at 10^6 K , is at most 170 km s^{-1} , irrespective of the composition of the gas. Thus $V_{\text{rel}}/V_{\text{rms}} \gg 1$, so the gas is strongly shocked, and its temperature is

$$T_{\text{shock}} \simeq \frac{3\mu m_{\text{H}}}{16k} V_{\text{rel}}^2,$$

where μ is the mean atomic weight of the gas, m_{H} is the mass of a H atom, and V_{rel} is the relative velocity (likely $\gtrsim 1000 \text{ km s}^{-1}$). Thus $kT_{\text{shock}} \sim 2 \text{ keV}$, more than adequate to account for both the presence of high-ionisation species and the high temperature implied by the Si lines (at least $10^{6.45} \text{ K}$, $\sim 3 \times 10^6 \text{ K}$, $kT \gtrsim 270 \text{ eV}$). Interestingly, this is significantly higher than the coronal gas temperature inferred in other novae, e.g., $10^{5.5} \text{ K}$ (several novae; Greenhouse et al. 1990), $10^{6.2} \text{ K}$ (RS Oph; Banerjee et al. 2009), $10^{5.6} \text{ K}$ (V1674 Her; Woodward et al. 2021), $10^{6.0} \text{ K}$ (V3890 Sgr; Evans et al. 2022), $10^{5.8} \text{ K}$ (U Sco; Evans et al. 2023), and is possibly the highest coronal temperature recorded in a nova eruption.

The higher coronal temperature in LMC68 might offer a clue to the absence of metal lines in the NIR. The high temperature of the coronal gas leads to *collisional ionisation* of ions, so that the abundances of neutral species (such as C I, O I) are negligible, while species normally appearing in IR coronal spectra (such as [Ca VIII]) are ionised to even higher stages. Thus, the fractional abundances of the ions listed in Table 2 of Woodward et al. (2021) (and itemised throughout the present paper) all peak at temperatures below $10^{6.3} \text{ K}$,

Table 3. Properties of the highest stages of ionisation discussed in this paper. See text for definitions of T_* and $T_{1/2}$.

Ion	λ (μm)	IP [†] (eV)	kT_* (eV)	$kT_{1/2}$ (eV)
[S IX]	1.2523	329	137	278
[P VIII]	1.375, 1.7361	264	110	223
[Si X]	1.4305	351	146	297
[Si XI]	1.9320	401	167	339
[Al IX]	2.0400	285	119	241
[Ca VIII]	2.3211	127	53	107

[†]Ionisation potential of lower stage.

their abundances diminishing at higher temperatures (see the tabulations in Arnaud & Rothenflug 1985).

For the species discussed in this work, the ionisation potentials of the ions that have higher stages of ionisation are listed in Table 3. These are generally less than that of Si IX (351.1 eV), and so lower ionisation stages of these ions are unlikely to exist in a gas having temperature $\gtrsim 10^{6.45} \text{ K}$; they have been ionised to higher stages by collisional ionisation. By analogy with the definition of kT_* , we define $T_{1/2}$ as the temperature of the Maxwellian gas in which at least half of the electrons are capable of ionising the lower ionisation stage ($kT_{1/2} \simeq 0.845 \times$ ionisation potential). Values of both kT_* and $kT_{1/2}$ are listed in Table 3. While the X-ray source is incapable of the necessary ionisation, a gas at $kT \gtrsim 270 \text{ eV}$ is certainly capable; note that this value is generally comparable with, or exceeds, the $kT_{1/2}$ values in Table 3.

The absence of almost all of the commonly observed metal lines in the NIR spectrum of nova LMC68 may therefore be a consequence of the unusually high temperature of the coronal gas, compounded by the expected underabundance of Mg and Ca in a TNR from a metal-deficient fuel. It may also account for the change in the NIR spectrum we observed between days 8.58 and 22.49. Furthermore, this change may also be consistent with the decline in the ultraviolet line flux reported by Shore et al. (1991) during the first week of the 1990 eruption.

7 CONCLUSION

We have presented the first NIR spectra of an extragalactic recurrent nova (OGLE 2016-NOVA-1, LMC V1341, LMCN 1968-12a) in eruption. The spectra, obtained 8.58 and 22.49 days after the eruption, are remarkable in that they are almost devoid of metal lines, with the sole exception of [Si X] 1.4305 μm line, which was extraordinarily strong on day 8.58.

We suggest that the absence of other metal lines in the NIR is a consequence of (a) the exceptionally high temperature of the coronal gas, resulting in the collisional ionisation of ions normally seen during the coronal phase of novae to even higher states of ionisation, so that the abundances of the states normally observed in the coronal gas are almost negligible, and (b) the underabundance of Mg and Ca in a metal-deficient gas that has been processed through a TNR. However, to better quantify this conclusion, it will be necessary to model the products of a RN TNR for systems having secondary stars with LMC abundances.

DATA AVAILABILITY

The raw infrared data in this paper are available from the Gemini Observatory Archive, <https://archive.gemini.edu/>.

The Magellan data will be made available on reasonable request to the first author.

The Swift data are available from https://www.swift.ac.uk/swift_live/ and <https://heasarc.gsfc.nasa.gov/cgi-bin/W3Browse/w3browse.pl>.

VISTA data are available at the European Southern Observatory Science Archive <http://archive.eso.org/cms.html>.

ACKNOWLEDGEMENTS

We thank the referee for their helpful comments on an earlier version of this paper.

The Gemini observations described in this paper were made possible through the award of Director's Discretionary Time GS-2024B-DD-104. The international Gemini Observatory is a program of NSF's NOIRLab, which is managed by the Association of Universities for Research in Astronomy (AURA) under a cooperative agreement with the National Science Foundation, on behalf of the Gemini Observatory partnership: the National Science Foundation (United States), National Research Council (Canada), Agencia Nacional de Investigación y Desarrollo (Chile), Ministerio de Ciencia, Tecnología e Innovación (Argentina), Ministério da Ciência, Tecnologia, Inovações e Comunicações (Brazil), and Korea Astronomy and Space Science Institute (Republic of Korea).

AP acknowledges prior support by a Carnegie Fellowship through which the Magellan time observing time was awarded. KLP acknowledges funding from the UK Space Agency. SS acknowledges partial support from a NASA Emerging Worlds grant to ASU (80NSSC22K0361) as well as support from his ASU Regents' Professorship.

REFERENCES

- Anupama G. C., 2008, in RS Ophiuchi (2006) and the Recurrent Nova Phenomenon, *Astronomical Society of the Pacific Conference Series*, eds A. Evans, M. F. Bode, T. J. O'Brien, M. J. Darnley, vol. 401, p. 31, San Francisco
- Arnaud M., Rothenflug R., 1985, *A&AS*, 60, 425
- Asplund M., Amarsi A. M., Grevesse N., 2021, *A&A*, 653, A141
- Badnell N. R., et al., 2006, in *IAU Symposium 234, Planetary Nebulae in our Galaxy and Beyond*, ed. M. J. Barlow & R. H. Méndez (Cambridge: Cambridge University Press), 211
- Banerjee D. P. K., Das R. K., Ashok N. M., 2009, *MNRAS*, 399, 357
- Banerjee D. P. K., et al., 2024, *ATel* #16771
- Benjamin R. A., Dinerstein H. L., 1990, *AJ*, 100, 1588
- Breeveld A. A., Landsman W., Holland S. T., Roming P., Kuin N. P. M., Page K. L., 2011, in *Gamma Ray Bursts*, ed J. E. McEnery, *American Institute of Physics Conference Proceedings*, Vol. 1358, 373
- Chen H.-L., Woods T. E., Yungelson L. R., Piersanti L., Gilfanov M., Han Z., 2019, *MNRAS*, 490, 1678
- Cioni M.-R., et al., 2011, *A&A*, 527, 116
- Cole A. A., Smecker-Hane T. A., Gallagher J. S., 2000, *AJ*, 120, 1808
- Darnley M. J., Henze M., 2020, *Adv. Sp. Res.*, 66, 1147
- Darnley M. J., 2021, in *The Golden Age of Cataclysmic Variables and Related Objects V*, *Proceedings of Science*, available online at <https://pos.sissa.it/cgi-bin/reader/conf.cgi?confid=368>, id. 44 (accessed 2024 November 29)
- Darnley M. J., Kuin N. P. M., Page K. L., 2024, *ATel* #16752
- Eikenberry S. S., et al. 2004, *SPIE*, 5492, 1196
- Evans A., Geballe T. R., Woodward C. E., Banerjee D. P. K., Gehrz R. D., Starrfield S., Shahbandeh M., 2022, *MNRAS*, 517, 6077
- Evans A., et al., 2023, *MNRAS*, 522, 4841
- Gehrels N., et al., 2004, *ApJ*, 611, 1005
- Gehrz R. D., et al., 2018, *ApJ*, 858, 78
- Greenhouse M. A., Grasdalen G. L., Woodward C. E., Benson J., Gehrz R. D., Rosenthal E., Skrutskie M. F., 1990, *ApJ*, 352, 307
- Healy-Kalesh M. W., Darnley M. J., Shara M. M., 2024, *MNRAS*, 528, 3531.
- Hummer D. G., et al., 1993, *A&A*, 279, 298
- Hsiao E. Y., et al. 2019, *PASP*, 131, 014002
- José J., García-Berro E., Hernanz M., Gil-Pons P., 2007, *ApJ*, 662, L103
- Kovetz A., Prialnik D., Shara M. M., 1988, *ApJ*, 325, 828
- Kuin N. P. M., et al., 2020, *MNRAS*, 491, 655
- Kumar V., et al., 2022, *MNRAS*, 510, 4265
- Liller W., 1990, *IAUC* 4964
- Mróz P., et al., 2014, *MNRAS*, 443, 784
- Mróz P., Udalski A., 2016, *ATel* #8578
- Page K. L., Kuin N. P. M., Darnley M. J., 2020, *ATel* #13731
- Page K. L., Kuin N. P. M., Darnley M. J., 2024, *ATel* #16772
- Pietrzyński G., et al., 2019, *Nature*, 567, 200
- Raj A., et al., 2015, *AJ*, 149, 136
- Rudy R. J., Russell R. W., Sitko M. L., Lynch D. K., Woodward C. E., 2024, *RNAAS*, 8, 199
- Simcoe R. A., et al. 2008, *Proc. SPIE*, 7014, 70140U
- Shore S. N., et al., 1991, *ApJ*, 370, 193
- Shore S. N., Charbonnel S., Garde O., Le Du P., Mulato L., Petit T., 2024, *ATel* #16761
- Skrutskie M. F., et al., 2006, *AJ*, 131, 1163
- Starrfield S., Schwarz G., Truran J. W., Sparks W. M., 2000, in *American Institute of Physics Conference Proceedings*, 522, 379
- Starrfield S., Iliadis C., Timmes F. X., Hix W. R., Arnett W. D., Meakin C., Sparks W. M., 2012, *BASI*, 40, 419
- Storey P. J., Hummer D. G., 1995, *MNRAS*, 272, 41
- Stubbings R., 2024, *vsnet-alert* 28015
- Wagner R. M., Depoy D. L., 1996, *ApJ*, 467, 860
- Warner B., 2012, in *Classical Novae*, eds M. F. Bode, A. Evans, p. 16, Cambridge University Press
- Woodward C. E., Banerjee D. P. K., Geballe T. R., Page K. L., Starrfield S., Wagner R. M., 2021, *ApJ*, 922, L10

This paper has been typeset from a \TeX/L\AA\TeX file prepared by the author.